UV aerosol absorption experiment (2002-04): 1. UV-MFRSR calibration and performance at GSFC

N.A. Krotkov[*a], P.K. Bhartia[b] and J.R.Herman[b], Jim Slusser[d],

Gwen Scott[d], G. Labow[c], T. F. Eck[a], and B. N. Holben[b]

[a]Goddard Earth Sciences and Technology Center Univ. of Maryland Baltimore County, MD USA;

[b]NASA Goddard Space Flight Center, Greenbelt, MD USA;

[c]Science Systems and Applications, Inc., Lanham, MD USA 20706

[d]USDA UVB Monitoring Network and Colorado State University

[*] Krotkov@chescat.gsfc.nasa.gov; phone 1 301 614-5553; fax 1 301 614-5903; http://toms.gsfc.nasa.gov; GEST Center, NASA/GSFC Code 916 Greenbelt, Maryland 20771

ABSTRACT

To reduce uncertainties in cloud-free sky UV radiative transfer models of the atmosphere, we conducted an aerosol UV absorption closure experiment where a shadow-band radiometer (a UV-MFRSR, USDA UVB Monitoring and Research Network) and a rotating group of four sun-sky CIMEL radiometers (part of NASA AERONET network) were run side-by-side continuously for 17 months at NASA/GSFC site in Greenbelt, MD. This paper describes a UV-MFRSR on-site calibration method based on AERONET CIMEL measurements of aerosol extinction optical thickness (t_{ext}) by direct a sun technique and Langley Mauna Loa calibrations. The AERONET t_{ext} was interpolated or extrapolated to the UV-MFRSR wavelengths and measurement intervals and used as input to the spectral band model along with column ozone and surface pressure measurements to estimate zero air mass voltages, V_o in each UV-MFRSR channel. The method does not require stability of t_{ext} and allows independent V_o estimations for every individual 3-min UV-MFRSR measurement. Daily $<V_o>$ estimates were obtained for cloud-free conditions and compared with the on-site Langley plot technique. On the clearest stable days both techniques agree within 1%. Uncertainties in t_{ext} measurements were estimated using co-located identical CIMEL instruments and considered as part of combined V_0 error budget. Such comparisons provide an independent check of both instrument's calibration, and allow relative tracking of the UV-MFRSR diffuser changes (from surface contamination), by repeating the comparisons on clear days. Using such comparisons we found relatively good daily UV-MFRSR $<V_0>$ reproducibility in summer (+/-2% in $<V_0(368)>$), but larger than expected $<V_0>$ relative changes in fall-winter seasons. The changes include systematic day-to-day $<V_0>$ decline for extended periods (with ~0.15%/day V_0 decline rate) alternating with step jump changes after major precipitation periods (rain or snow). The $<V_0>$ changes were highly correlated in all UV-MFRSR channels, and possibly result from diffuser contamination and cleanings. Daily $<V_0>$ values were used to calculate t_{ext} for 3-minute UV-MFRSR measurements. These results compared well with interpolated AERONET t_{ext} measurements (at 368nm daily rms differences in t_{ext} were within 0.01 (1σ) for $\tau_{ext}< 0.4$ and within 0.02(1σ) for $\tau_{ext}<1.2$). The advantage of the shadowband technique is that the $<V_0>$ calibration obtained for direct-sun voltage can be applied to diffuse and total voltages to obtain total and diffuse atmospheric transmittances. These transmittances, in combination with accurate t_{ext} data, provide an essential foundation for the aerosol column absorption retrievals described in the second part of this paper.

Keywords: ultraviolet radiation, aerosol absorption, single scattering albedo, CIMEL sun photometer, AERONET network, UV multi-filter rotating shadow band radiometer, UV-MFRSR, diffuse fraction measurements, Langley calibration

1. INTRODUCTION

Improved knowledge of aerosol absorption properties in the near UV is needed for modeling of tropospheric chemistry because it affects the calculated rate of photochemical reactions[1,2] and smog production[3] as well as penetration of biologically harmful UV radiation to the surface[4-13]. Changes in aerosol amount may enhance, reduce or even reverse UV radiation effects of stratospheric ozone changes. The global average ozone reduction was less than 5% for the past 20 years, and ozone is expected to recover slowly over next 20-50 years. At one of the biologically important wavelengths, 310 nm, each 1% column ozone decrease produces approximately ~1% UV increase. Radiative transfer (RT) calculations show that decreases in UV due to moderate increases in absorbing aerosol amounts are comparable to that caused by stratospheric ozone recovery with one important difference. Aerosols affect both UVB (280 to 320 nm) and UVA (320 to 400 nm), while ozone sensibly only affects UVB. Therefore, conducting measurements in both spectral regions allow separation of ozone and aerosol effects on surface UV irradiance.

Aerosols may be changing the rate of tropospheric ozone formation caused by sunlight, NOx and urban smog, but the magnitude and even the sign of the aerosol effect is currently highly uncertain. Scattering by aerosols can actually increase actinic flux above the aerosol layer, as well as the rates of photochemical reactions in the upper parts of the planetary boundary layer[1-3], while aerosol absorption reduces the amount of UV radiation available for chemical reactions. The combined aerosol effect on smog production depends not only on the total aerosol loading, but also on the aerosol vertical distribution and its absorption properties. If aerosol UV absorption is indeed strong enough to suppress photochemical smog production, then reduction in soot emissions in the developing world may make the smog problem worse in the short-term unless accompanied by reductions in other pollutants.

Although it is well known that iron oxides in desert dust[37] and soot produced by fossil fuel burning and urban transportation strongly absorb the UV radiation, properties of other potential UV absorbers, e.g., nitrated and aromatic aerosols[5], are poorly known. Ground based remote estimates of column aerosol absorption in UV are sparse and not yet validated[6,7,10,13]. The lack of validated aerosol absorption measurements in UV makes it difficult to quantify the reason for an observed discrepancy in modeled and measured UV irradiances[14] and photolysis rates.

To reduce current uncertainties in RT model inputs we conducted an aerosol UV absorption closure experiment where a shadow-band radiometer (UV-MFRSR, USDA UVB Monitoring and Research Network) [15-17] and several CIMEL sun-sky radiometers (part of the NASA AERONET network) [18,19] were run side-by-side continuously for 17 months at NASA/GSFC site in Greenbelt, MD. First, we briefly describe instrumentation and datasets used in this study. This is followed by a detailed description of UV-MFRSR operating procedures, raw voltage corrections and estimated measurements uncertainties. Section 3 discusses a new UV-MFRSR spectral band model used to calibrate UV-MFRSR direct voltage measurements and calibration results. The calibration technique is validated by comparisons with Langley plots and AERONET aerosol extinction optical thickness, t_{ext}, obtained by the direct-sun technique and Mauna Loa Langley calibration.

The UV-MFRSR calibration obtained for the direct-sun voltage $<V_0>$ is directly applicable to diffuse and total voltage measurements, which allows us to infer aerosol absorption optical thickness. The aerosol absorption results of our measurements are presented in a follow-up paper.

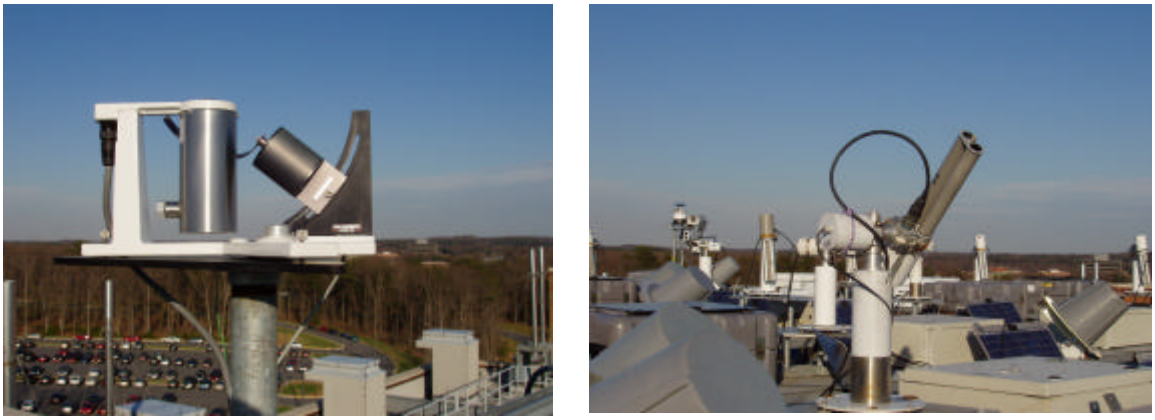

Figure 1.*UV-MFRSR instrument (left) and CIMEL sun/sky photometer (right) were run side by side at NASA Goddard Space Flight Center in Greenbelt, Maryland in 2002-2003. The height of elevated platform at the roof of the building is ~20m above ground (~100m above sea level).*

2. Instrumentation

The UV-MFRSR (Figure 1, left) is a shadow-band instrument that measures diffuse and total horizontal radiation[16]. The USDA UVB Monitoring and Research Network currently operate 31 of these instruments continuously[15] at sites distributed across the US. These instruments are capable of retrieving column ozone[28], aerosol optical thickness[17], and calibrated diffuse and direct irradiance. A single measurement cycle consists of measuring total horizontal irradiance (no sun blocking) following by 3 irradiance measurements with different positions of the shadow band blocking the sun and aureole on each side of the sun. The complete cycle takes ~10sec and is repeated every 3 minutes throughout the day. All spectral channels are measured within one second by 7 separate solid-state detectors sharing a common Teflon diffuser[16]. The raw data (voltages) are automatically transmitted (via dedicated telephone modem) to the USDA UVB network processing center at the Colorado State University (Fort Collins, CO) for calibration and further processing. The standard UVB network data processing includes calculation of diffuse horizontal and direct-normal components of the irradiance based on NOAA Central Ultraviolet Calibrations Facility (CUCF) measured spectral and angular response functions and applying absolute radiometric (lamp) calibration to all irradiance components. Subsequent monthly re-processing includes Langley on-site calibration checks on clear days using the Harrison and Michalsky algorithm[17] and calculation of aerosol optical thickness and column ozone (all standard data available at http://uvb.nrel.colostate.edu/UVB/home_page.html).

Direct sun aerosol optical thickness measurements reported in this paper were made with CIMEL Sun-sky radiometers (Figure 1, right), which are a part of the AERONET global network (data

available at http://aeronet.gsfc.nasa.gov). While these instruments are described in detail by *Holben et al*[18,19], a brief description will be given here. The automatic tracking Sun and sky scanning radiometers make direct Sun measurements with a 1.2^0 full field of view every 15 min at 340, 380, 440, 500, 675, 870, 940, and 1020 nm (nominal wavelengths). The direct Sun measurements take 8s to scan all 8 wavelengths, with a motor-driven filter wheel positioning each filter in front of the detector. These solar extinction measurements are then used to compute aerosol optical depth at each wavelength except for the 940 nm channel, which is used to retrieve total precipitable water. The filters utilized in both instruments were ion-assisted deposition interference filters with band pass (full width at half maximum) of the 340 nm channel at 2 nm and the 380 nm filter at 4 nm, while the band pass of all other channels was 10 nm. The AERONET data we present here were quality- and cloud-screened following the methodology of Smirnov et al[30].

Ancillary measurements at our site include Brewer double monochromator column ozone measurements (Figure 2) and surface pressure measurements from nearby USDA Beltsville location corrected for the altitude differences (Figure 3).

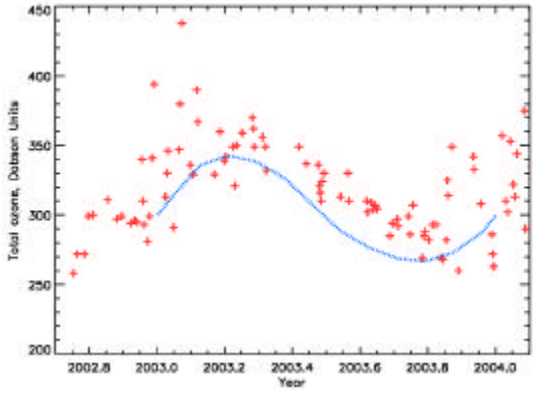

Figure 2 *Brewer column ozone measurements at GSFC site on cloud-free days in 2002-2004. Thin blue line shows climatological mean ozone values from London et al.*[36] *assumed in AERONET processing.*

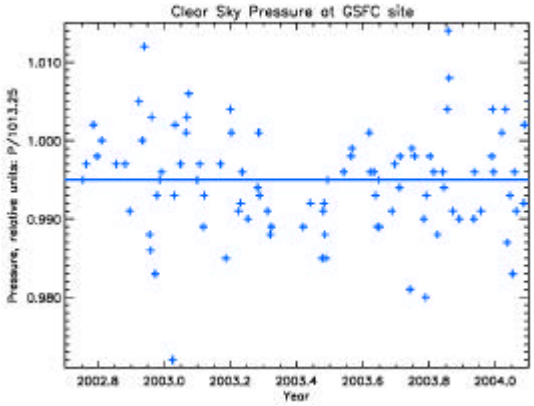

Figure 3 *Daily average pressure measurements from USDA Beltsville location corrected for altitude differences with NASA GSFC (4mb constant offset). The annual mean pressure is 0.995atm (1 atm=1013,25mbar) with ~3% peak to peak to peak variations.*

3. UV-MFRSR Operating Procedures and Calibration

3.1. UV-MFRSR installation at GSFC site

One UV-MFRSR instrument of the UVB USDA network was installed at the AERONET primary calibration site at NASA Goddard Space Flight Center (GSFC) in Maryland with routine operation started on October 1, 2002. The instrument's location on an elevated platform on the roof of a building allows an unobstructed view of the horizon (Figure 1). The special bubble level we use to fine tune the level allows adjustment to about 10 arc minutes. The motor was adjusted until the drive shaft angle is within ~ 0.2^o of the latitude. Finally we manually slip the band (and/or adjust it in software) so that the band shadow is centered over the diffuser at each cycle during the entire day. This shadowing adjustment was initially done during installation on October 1, 2002 within one hour of solar noon, but also manually checked throughout routine operation and adjusted if necessary. These adjustments allow correct tracking of the shadowband all day and throughout the year.

3.2 Raw voltage corrections

As described by Harrison et al. [16], the UV-MFRSR instrument measures total horizontal and diffuse horizontal irradiances in terms of detector voltages. Within the instrument's data logger, the direct normal voltage is determined by subtraction of the diffuse component from the total and normalizing by cosine of the solar zenith angle. The raw total, diffuse and direct normal voltages are transferred to USDA UVB center via dedicated modem line for further processing.

Nighttime bias (dark current) voltages are first subtracted from the diffuse horizontal voltages by the following procedure: a) determining the time of minimum solar elevation during the previous 1-3 days; b) averaging the nighttime bias readings from 1 hour prior to 1 hour after the time of minimum solar elevation; and c) subtracting the average bias from measured diffuse voltage (if more than 1mv). For this study, the average daily bias subtracted from the voltages measured at 368 nm was 1.71 mV (σ=0.552). Bias correction is unnecessary for the other components since the direct component is effectively corrected during the subtraction in the data logger and the total horizontal voltage is recalculated as explained below.

Angular corrections are then applied to the direct normal voltages to compensate for the instrument's deviation from ideal (cosine) angular response. Figure 4 shows actual angular response functions used to correct the measured voltages for the 368 nm channel. Angular response factors for the diffuse voltages, $f_D(l)$, are determined using the isotropic sky assumption as described in Leszscynski et al[33]. The diffuse, nighttime bias-corrected horizontal voltage is divided by the diffuse angular correction factor, which, for this study, was 0.9927 for the 368 nm channel. Experimental measurements of the actual sky radiance distribution in UV and Visible had shown that an isotropic assumption underestimates the actual diffuse cosine error up to 10% at 500nm, 6% at 400nm, 4% at 350nm ~ 2% at 320nm depending on sky inhomogeneity factor[34]. We

note however, that diffuser optics of the instrument used in that study deviates significantly from the ideal cosine response (f_D(isotropic)~0.88). On the other hand, the diffuser geometry for the UV-MFRSR instruments was specifically designed to compensate for cosine errors[16] so that f_D(*isotropic*)~0.99 at 368nm for our instrument. Thus, we conservatively assume ~0.5% uncertainty in f_D*(isotropic)* at 368nm due to unaccounted sky inhomogeneity. We also note that sky radiance becomes more isotropic at shorter UV wavelengths, so the error in f_D*(isotropic)* gets even smaller at shorter wavelengths UV-MFRSR channels.

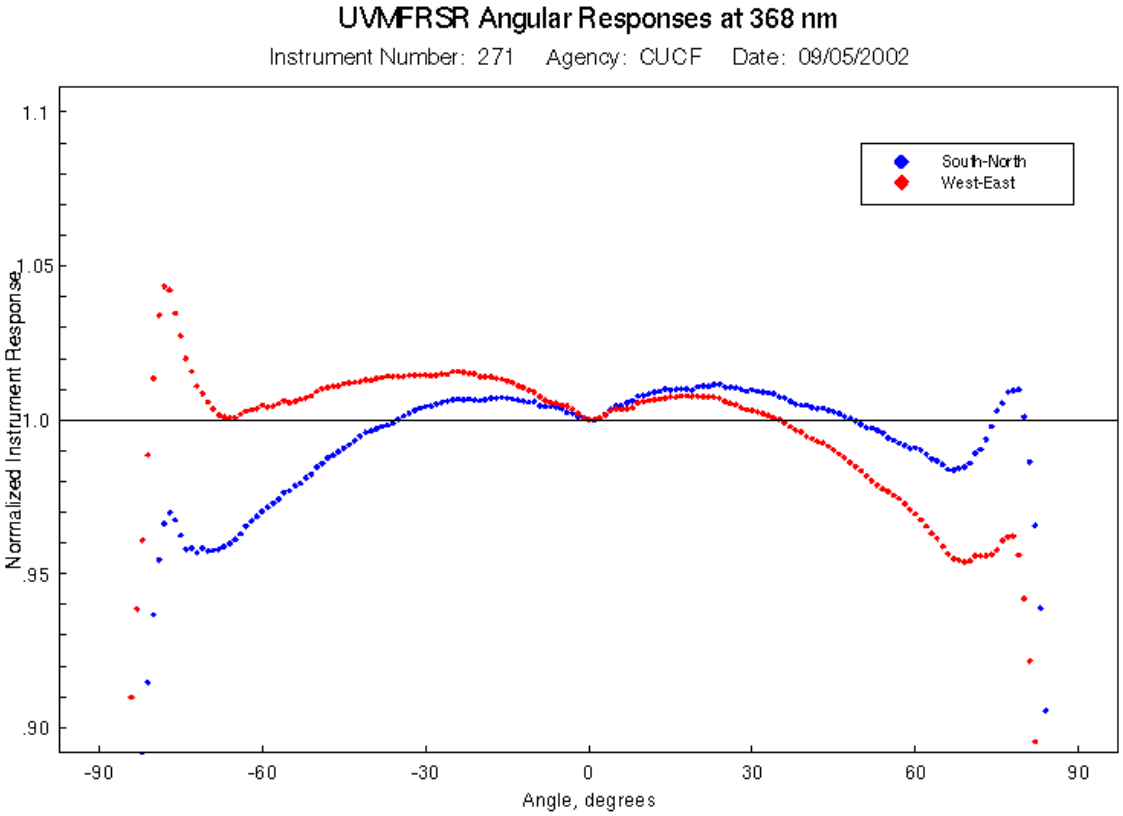

Figure 4 *UV-MFRSR angular response function, normalized to the ideal (cosine) angular response(f_R=1 for ideal instrument). Instrument head #271, at 368nm measured by CUCF on 5 September 2002 before deployment at GSFC site. For each of the 7 channels, there are 2 sets of responses: one from the south to north scan (labeled SN), and one from the west to east scan (WE). Correction factor of the measured direct-normal voltage, f_R, is interpolated according to solar zenith and azimuth angles at the time of actual measurement. The azimuth angle, j (0^o-359^o), is resolved into the four quadrants and normalized angular response factor for direct voltage, f_R, is calculated as described by Harrisosn and Michalsky*[16].

Finally, the total horizontal voltage, V_T, is re-calculated by summing the cosine corrected direct normal voltage (converted back to horizontal) and the dark current and diffuse horizontal voltage

corrected for angular response. The whole process can be described using single correction factor for total irradiance, f_T in each channel: $V_T(corrected) = V_T^{Meas} / f_T$:

$$\frac{1}{f_T} = \frac{1 - DT^{Meas}}{f_R} + \frac{DT^{Meas} - \frac{V_{Dark}}{V_T^{Meas}}}{f_D(isotropic)} \qquad (1)$$

where DT^{Meas} is measured (raw) diffuse to total voltage ratio, f_R is given by equation (1) and $f_D(isotropic)$~0.99 at 368nm. The USDA UVB Monitoring and Research Program reports the corrected voltages, on its Web site (http://uvb.nrel.colostate.edu/UVB/home_page.html) as "angular (cosine) corrected data." Furthermore, it is these direct normal voltages that are input to the Langley analysis described by Harrison and Michalsky[17]. Estimated errors associated with the voltage corrections applied and combined errors in $V_T(corrected)$ are shown in Table 1.

3.3 UV-MFRSR on-site calibration

Assuming UV-MFRSR's radiometric sensitivity remains a constant linear function (i.e. doubling the input irradiance results in doubling the output voltage, V_n), one only needs to know V_{no} (instrument voltage for direct solar flux extrapolated to the top of the atmosphere) to derive atmospheric transmittance directly from the voltage measurement. The same V_o is applied to direct and diffuse voltages, since both are measured by the same diffuser/filter/detector combination. Therefore, our on-site calibration strategy includes the following main steps:

1) Develop UV-MFRSR spectral band model to calculate direct atmospheric transmittance, T_R, in each UV-MFRSR spectral channel given auxiliary measurements of aerosol extinction, t_a,(interpolated from AERONET CIMEL direct sun measurements), molecular (Rayleigh) scattering amount, $t_R P$ (P is relative atmospheric pressure, P/P_{std}, P_{std}=1013.25mbar) and gaseous (ozone) absorption, t_{O3} (see Table 1 and Figure 5);
2) Calculate effective Vo for each individual measurement of direct-normal voltage, Vn and calculated T_R using equation (2); obtain daily average calibration factor, $<Vo>$
3) Calculate radiatively equivalent wavelength, l_{rad}, and aerosol optical thickness $t_{ext}(l_{rad})$ using Vn, $<Vo>$ and subtracting of Rayleigh and ozone contributions. We also need to know l_{rad} to correctly partition t_{ext} between different atmospheric processes in calculating diffuse irradiance component (described in 2nd part of the paper).
4) Calculate total and diffuse transmittances by normalizing corresponding voltages by $<Vo>$;
5) Calculate aerosol absorption optical thickness from $t_{ext}(l_{rad})$ and either diffuse of total transmittance (described in 2nd part of the paper).

Our spectral band model (Figure 5, Table 2) takes into account actual UV-MFRSR spectral response functions (SRF) as well as spectral variation of the solar flux and atmospheric extinction

within each filter bandpass of the instrument. We derive individual V_0 by numerically integrating high resolution spectral transmittance $T_R(\lambda)$ within each filter bandpass:

$$T_R(\lambda) = e^{-m(t_a(\lambda_{nrad})+t_R(\lambda_{nrad})+t_{O3}(\lambda_{nrad}))} = \frac{\int_{\lambda_{n\min}}^{\lambda_{n\max}} E_0(\lambda)F(\lambda)e^{-m(t_a(\lambda)+t_R(\lambda)P+t_{O3}(\lambda))}d\lambda}{\int_{\lambda_{n\min}}^{\lambda_{n\max}} E_0(\lambda)F(\lambda)d\lambda} = \frac{V_n}{V_0} \quad (2)$$

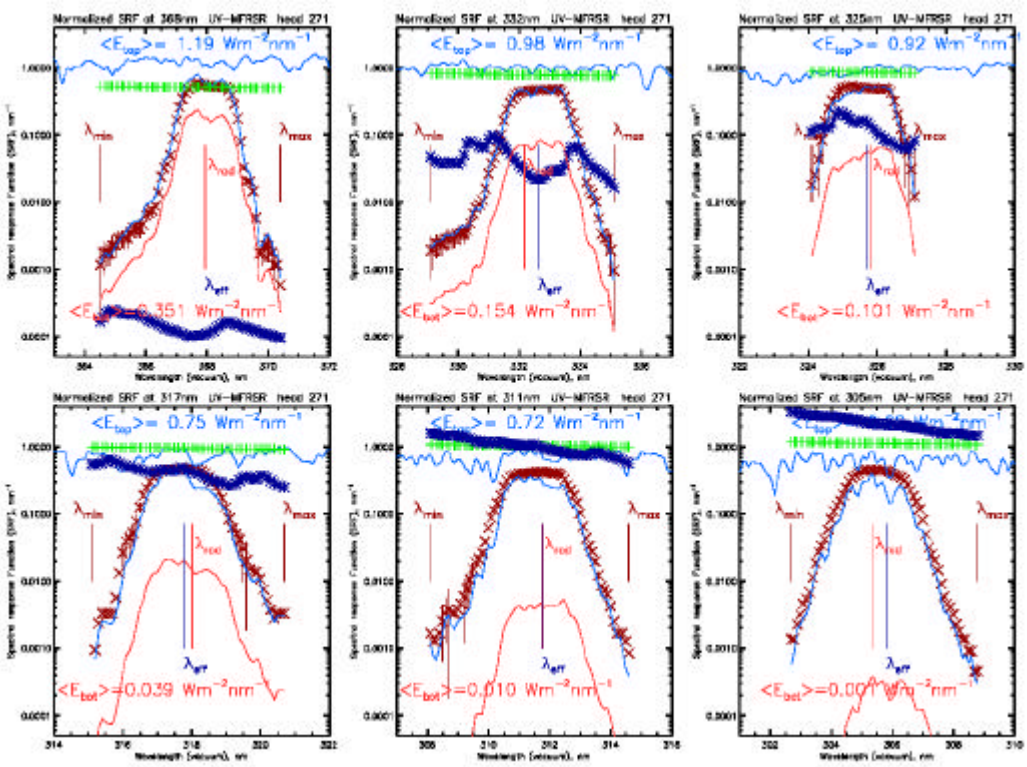

Figure 5 *Example of UV-MFRSR high-resolution spectral band model. Spectral response functions (SRF) for UV-MFRSR # 271 were measured at CUCF in September 2002 before instrument's deployment at GSFC site (red crosses with estimates of error bars), ETS solar irradiance (blue curve) (SUSIM ATLAS-3 measurements), spectral Rayleigh optical thickness (green crosses) and spectral ozone optical thickness (purple crosses for 350DU column ozone amount and ozone weighted temperature –45C). Also shown is spectral direct normal irradiance convolved with SRF at the top of atmosphere (blue solid line) and at the surface (assuming 1 atm surface pressure, 500DU column ozone, aerosol optical thickness 0.1 at 368nm and angstrom parameter 1) along with spectral integral for each bandpass. To obtain a unique solution for λ_{dir} only values falling in the interval (λ_{neff} -0.5nm, λ_{neff} +0.5nm) are retained (see example in Table 2).*

In equation (2) the denominator represents absolute solar flux that would be measured by UV-MFRSR at the top of the atmosphere, while numerator represents attenuated solar flux measured at the surface. To evaluate the integrals one needs to know the extraterrestrial solar flux, E_0, normalized spectral response function, F (l_{min} , l_{max} are channel cutoff wavelengths), atmospheric spectral extinction optical thickness and relative airmass factor, m. The UV-MFRSR spectral response functions (SRF) for all channels are shown in figure 5 and the spectral band model is given in Table 2 for a nominal aerosol model. In practice, we use AERONET interpolated/extrapolated t_a to calculate $T_R(l)$ within each bandpass and numerically evaluate spectral integral in (2). We also calculate the radiatively equivalent wavelength, l_{rad} defined by equation (2). Using $l_{rad,}$ we can re-write equation (2) in a linear form suitable for Langley regression:

$$\ln(V_0) = \ln(V_n) + m(t_a(l_{rad}) + t_R(l_{rad})P + t_{O3}(l_{rad})) \qquad (3)$$

To derive V_o from either equation (3) or (2) (calibration step (2)) we need to interpolate or extrapolate aerosol extinction optical thickness t_{ext} to a given l_{rad} using AERONET direct sun measurements as described in next section.

3.4. Spectral Extrapolation/Interpolation of AERONET direct-sun measurements

Only τ_{ext} measurements from AERONET-CIMEL reference instruments were used that were calibrated at the Mauna Loa Observatory (MLO) every 2-3 months using the Langley plot technique (Table 3)[35]. Therefore, the uncertainty in τ_{ext} due to the uncertainty in V_o for the reference instruments is better than 0.002-0.005 in the visible[18], but larger in UV. In operational AERONET processing there is no adjustment of Rayleigh optical depth for departure from mean surface pressure (P~0.994 atm. at GSFC). Since pressure variations from day to day can reach 0.03atm (Figure 2), which is not insignificant at UV wavelengths with high Rayleigh optical depth (Table 2), we corrected AERONET τ_{ext} data in the UV (340 nm and 380nm) for the actual atmospheric pressure at the time of measurement.

$$\Delta t_a(l,t) = t_R(l)[1 - P(t)/P_A] \qquad (4)$$

Here, t_R is AERONET standard Rayleigh optical thickness subtraction for specific instrument and channel (Table 3), adjusted to mean GSFC pressure, P_A (P_A =0.993769 atm), and $P(t)$ is actual pressure at time of measurement normalized to 1 atm = 1013.25mbar. The maximum $D\tau_{ext}$ due to atmospheric pressure variations (see figure 2) is ~0.01 at 340nm, while at 380 nm the correction is half of that amount and proportionately less at visible wavelengths. Additionally, in the computation of τ_{ext} for 340, 500, and 675 nm, ozone optical depth is also subtracted from total optical depth using climatological mean ozone values. Because of the small ozone absorption at these wavelengths, departures from climatological values by 50% (which are very large fluctuations) would result in additional uncertainty in computed τ_{ext} of only ~0.004 at 340 nm,

0.0045 at 500 nm, and 0.0063 at 675 nm. Again, these are the probable maximum departures caused by total column ozone variability. Typical departures would be less than half this magnitude (see figure 2). We compute the combination of calibration uncertainties of V_o and uncertainty in ozone and Rayleigh optical depth, for optical airmass of 1, in the manner of *Russell et al.*[37]. For our error budget we assume that uncertainties in ozone optical depths are equal to 1/3 of the maximum values given above. We therefore calculate an estimated total uncertainty of ~0.002-0.009 for a single CIMEL reference instrument at GSFC. If we take into account differences between reference CIMEL instruments in UV, the uncertainty increases to 0.01–0.02, which is significantly larger than the spectral interpolation uncertainty at 368nm and even typical extrapolation uncertainty at 325nm (Figure 6).

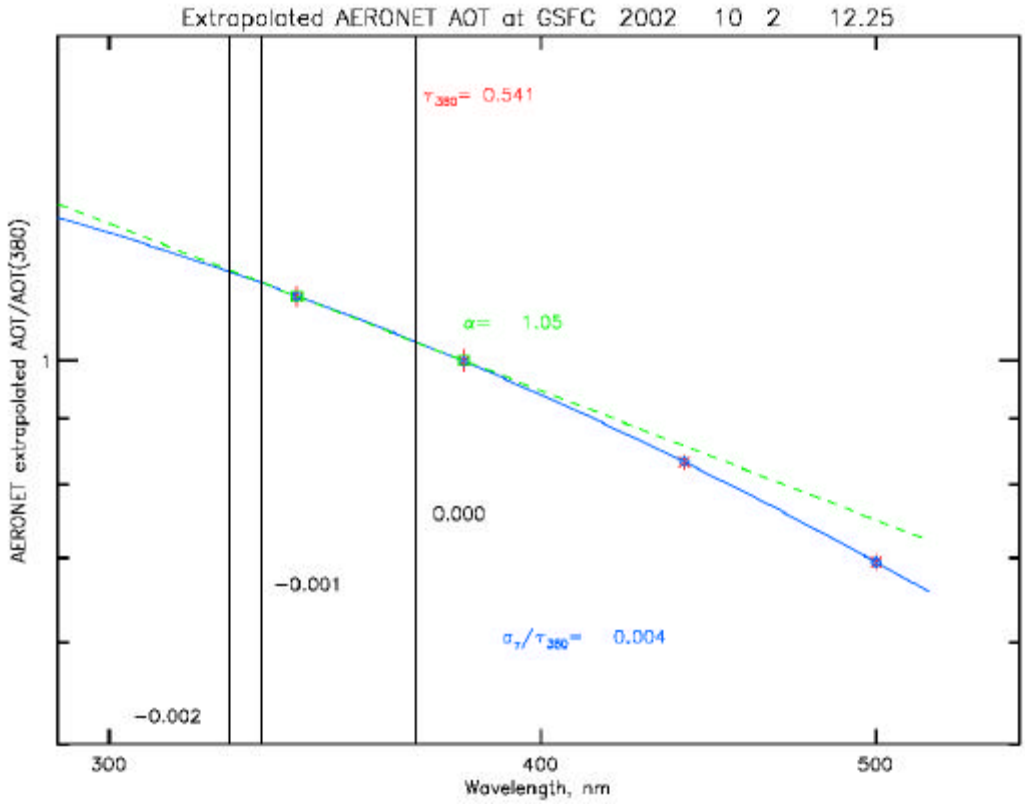

Figure 6. *AERONET direct sun aerosol extinction optical thickness at 340nm, 380nm, 440nm, and 500nm normalized by t(380). Extrapolation to longer UV-MFRSR channels using quadratic least squares fit of ln(t) versus ln(l) (solid line) and linear extrapolation of ln(t) versus ln(l) from 340nm and 380nm (dashed line). Absolute differences between 2 extrapolation methods are shown next to vertical bars representing centers of UV-MFRSR spectral channels. The difference in t_{ext} between interpolation methods is typically less than 0.005 at 368nm.*

We extrapolate or interpolate AERONET t_{ext} measurements at 340nm, 380m, 440nm, and 500nm to the UV-MFRSR wavelengths using a least squares quadratic fit in log-log space (Figure 6)[23]. One could also use linear extrapolation in log-log space (dashed curve in Figure 6) assuming that the Angstrom parameter does not change. Although this assumption obviously does not hold for large wavelength spans (~100nm), both methods provide practically identical results in the UVA spectral region (320nm - 400nm). In our calibration technique, we use both methods and discard extrapolated values if they differ more than 0.01. At 368nm we interpolate rather than extrapolate and both methods typically provide practically identical results (within 0.003, figure 6). Therefore, we feel that spectral extrapolation is a negligible source of error in our calibration technique for longer UV-MFRSR channels.

4. UV-MFRSR daily *Vo* Calibration Results

Figure 7 shows examples of daily V_0 calibration results at 368nm for cloud-free days with high (top panel) and low aerosol loadings (low panel). Standard deviation of V_o daily data, s_{lnV0}, provides an overall measure of atmospheric and instrumental variability on a given day and is directly related to the uncertainty in derived individual t_{ext} values. On the clearest days at GSFC the scatter in *Vo* can be quite small (s_{lnV0} ~0.006 for t_{ext}~0.1,figure 7, low panel), but the scatter increases on days with high turbidity (s_{lnV0} ~0.03 for t_{ext}~0.6, figure 7, upper panel). Calculating daily means of individual V_0 values reduces the effect of random errors for transferring the AERONET calibration by the square root of the number of available measurements. Typically there are ~60 daily V_0 estimates in winter compared to ~200 in summer, therefore, random error in estimating daily mean $<V_0>$ value (shown as a horizontal line in figure 7) is reduced by a factor 8 to 20. The effect of random errors was further reduced by removing outlier measurements (with $ln(V_0)$ outside of +/- $3s_{lnV0}$ of the $<ln(V_0)>$) and iteratively re-calculating $<V_0>$. We found that removing less than 5% of outliers reduces s_{lnV0} by half on both clear and turbid days (in figure 7 s_{lnV0} are shown for 3 iterations).

Examining diurnal trends in V_0 data provides insight into possible systematic calibration errors and yields a tool for checking consistency between AERONET-CIMEL t_{ext} and UV-MFRSR voltage measurements. Indeed, for perfect measurements, V_0 should remain constant during the day regardless of any changes in atmospheric conditions, solar elevation, and azimuth. For example, any systematic residual errors in UV-MFRSR cosine or shadowing corrections will manifest themselves as systematic $ln(V_0)$ changes with solar zenith angle. On the other hand, any constant error in AERONET extrapolated t_{ext} would produce errors in $ln(V_0)$ that are proportional to the airmass factor, m (see equation 3), and would result in a diurnal pattern in $ln(V_0)$ with systematic increase or decrease at high m depending on the sign of the t_{ext} error. For example, a small systematic decrease in $ln(V_0)$~0.015 can be seen on March 14, 2002 (figure 7, lower panel) in early morning and late evening at m~5. Assuming that all this decrease is due to extrapolation of t_{ext}, we could estimate upper limit of this error: Dt_{ext} ~0.015/5=0.003 (assuming the error remains constant during that day) that is within uncertainty of AERONET t_{ext} measurements. Thus, a longer calibration period permits a better estimate of possible systematic errors.

.

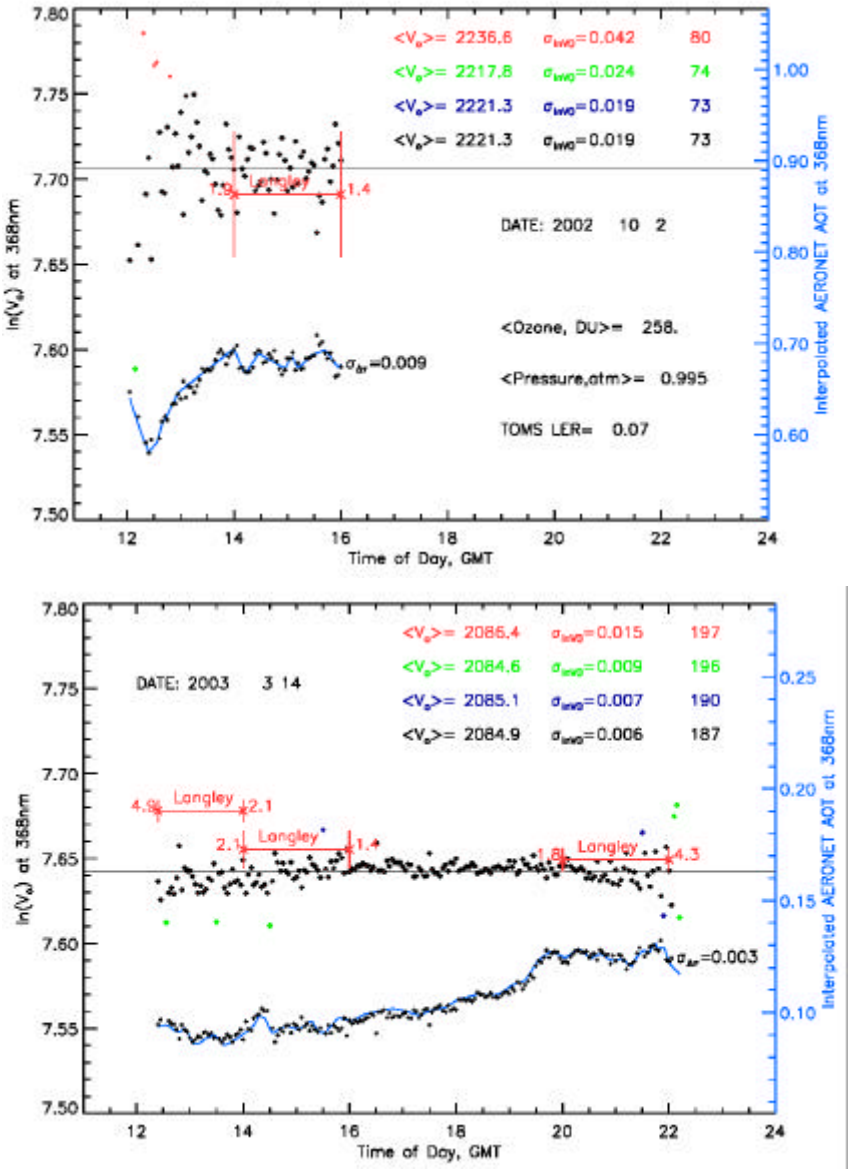

Figure 7. *Daily V_0 calibration curves on cloud-free days with high (top) and low aerosol loading (bottom). Points represent individual V_o estimates and horizontal line represents daily average V_o value after removing the outlier UV-MFRSR measurements outside of +/-3s_{lnVo} (3 iterations are shown in different colors). 2-hour Langley plot intercepts are represented as red horizontal lines with 1s_{Co} error bars and initial and final airmass values used in regression. Interpolated AERONET direct-sun t_{ext} is shown as blue line and calculated UV-MFRSR t_{ext} are shown as black crosses for each 3-minute measurement (with scale on the right). Daily rms differences between the AERONET and the UV-MFRSR t_{ext} are also shown on the right to the t_{ext} curves.*

There is a possibility that different systematic errors can compensate each other in such a way as to cancel any observable diurnal dependence in *ln(Vo)*, while still producing a bias in daily mean <*Vo*>. Therefore, an independent on-site calibration method is required to cross validate our calibration procedure. In perfectly stable atmospheric conditions the Langley plot calibration method would provide an ultimate check on the measurements, spectral band model and $<V_0>$ calibrations[17]. Standard Langley technique regresses $ln(V_n)$ versus *m*, so *ln(Vo)* is obtained as the zero airmass intercept of a linear regression model given by equation (3). This method does not require any a-priori knowledge of the atmospheric transmittance, beyond the stability requirement, which was difficult to meet at our site. Therefore, we tried to optimize standard Langley technique by adjusting the time interval used in regression to ensure maximum possible stability of t_{ext} during calibration. Figure 7 shows Langley technique C_o results (with $1 s_{Co}$ error bars) for different 2-hour calibration periods. We see that Langley technique produces close *Vo* results (within 1σ error bars), when t_{ext} ~*const*. The comparisons, although somewhat subjective, provide crucial evidence of the consistency between AERONET-CIMEL and the UV-MFRSR calibrations.

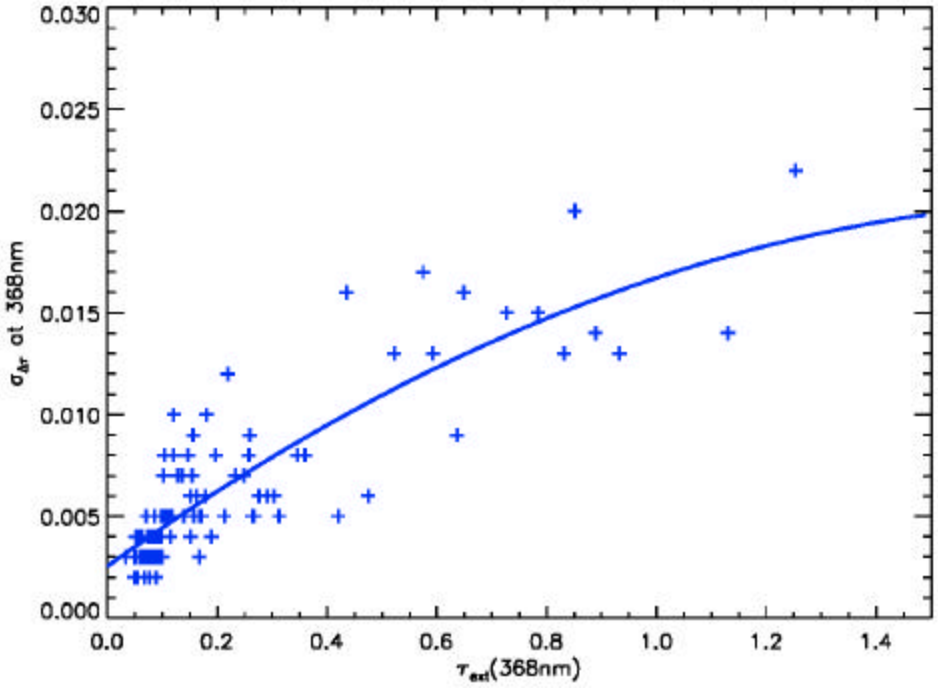

Figure 8. *Daily aerosol extinction optical thickness rms differences between UV-MFRSR and AERONET CIMEL measurements at 368nm.*

Finally, we calculated the optical thickness, t_{ext} for each individual UV-MFRSR V_n measurement (except outlier measurements, less than 5% see figure 7) using equation (3) and daily mean <*Vo*>

value and compared with AERONET extrapolated t_{ext}. Both instruments show excellent consistency in t_{ext} throughout the day with no obvious bias on turbid or clear days. Figure 7 shows that both t_{ext} measurements track each other perfectly with small scatter, which was well within uncertainties of AERONET t_{ext} measurements (daily rms differences in t_{ext} <0.01 on turbid days and ~0.003 on clear days). Figure 8 summarizes t_{ext} comparison results at 368nm for all cloud-free days of the whole observational period. We found an increase in daily rms differences with increase in atmospheric turbidity: daily *rms* differences in t_{ext} are within 0.01 ($1\,s$) for t_{ext}< 0.4 and within 0.02($1\,s$) for t_{ext}<1.2. Much of this increase can be attributed to a real increase in short-term atmospheric variability on turbid days, when time interpolation of 15minute AERONET measurements caused large errors in t_{ext}. The interpolation error was less important on clear days with low turbidity, when *rms* differences were ~0.002.

5. Long-term changes in UV-MFRSR V_o calibration

Comparisons of aerosol extinction optical thickness provided an independent check of both instrument's calibration and allowed relative tracking of the UV-MFRSR diffuser transmission changes (from surface contamination) by repeating the comparisons on clear days. Using such comparisons we found UV-MFRSR had relatively good daily $<V_0>$ reproducibility in summer (+/- 2% in $<V_0(368)>$), but larger than expected V_0 changes in fall-winter seasons (Figure 9).

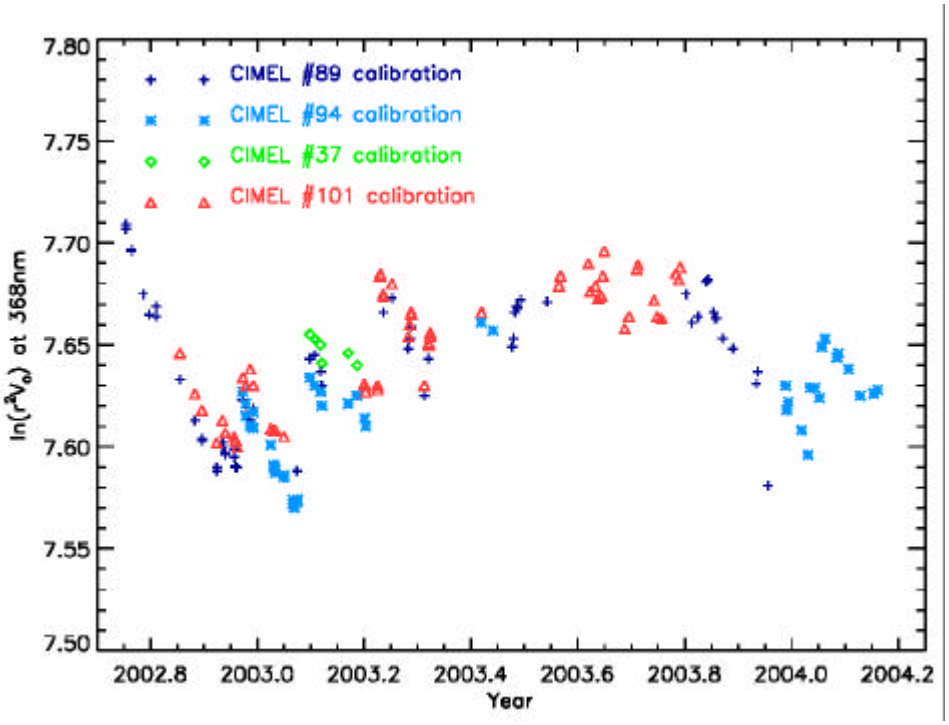

Figure 9. UV-MFRSR daily calibration results (normalized to Sun-Earth distance) at 368nm.

The changes include periods of systematic day-to-day V_0 decline for extended periods alternating with step jump changes after major precipitation periods (rain or snow). We repeated calibrations using different reference CIMEL instruments with essentially the same results (Figure 9). Maximal difference in $<ln(Vo)>$ on any given day was only ~0.02 from using different CIMELs for calibration. This is not enough to explain ~0.12 decrease in $<ln(Vo)>$ between October 1 December 17, 2002. The first upward ~4% step jump occurs between December 17, 2002 ($<ln(r^2Vo)>=7.59$) and December 21, 2002 ($<ln(r^2Vo)>=7.63$) and was probably caused by diffuser cleaning. After that event, $<ln(r^2Vo)>$ continued to decrease at the same rate (~0.15%/day) until January 27, 2003, when the largest upward step jump occur (~7%). The 3d step jump (+4%) had occurred between March 23 and 25 2003. Next, $<ln(r^2Vo)>$ stabilized until fall 2003 when a decline started again in September 2003 resembling the behavior in 2002.

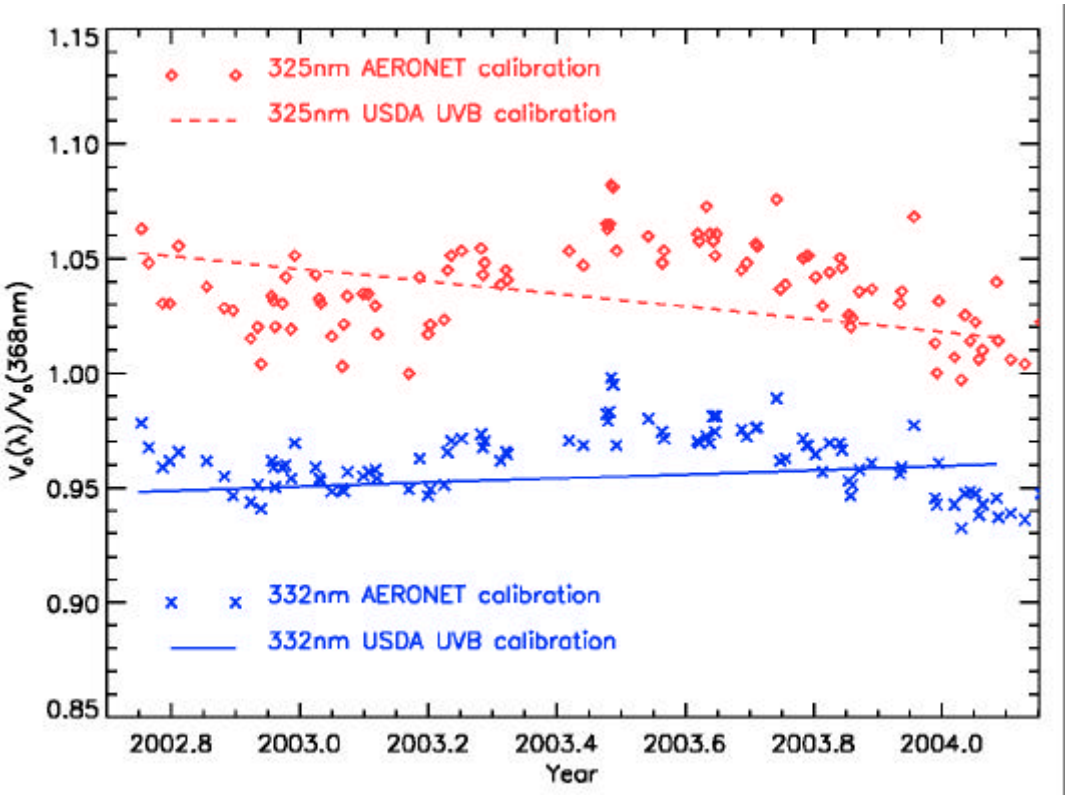

Figure 10. *Daily UV-MFRSR $<V_o(332nm)>$ and $<V_o(325nm)>$ calibrations, normalized to $<V_o(368nm)>$ calibration*

Since the day-to-day $<V_0>$ changes were highly correlated in all UV-MFRSR channels (figure 10), they are probably caused by real changes in the sensitivity of the whole instrument (not individual filters or detectors) or some external changes affecting on-site UV-MFRSR calibration procedure. Step jumps changes in $<Vo>$ can be related to changes in UV-MFRSR throughput caused by

diffuser contamination and cleanings. Before sending the UV-MFRSR optical head for post-deployment calibration, we did a test of diffuser contamination by not cleaning the diffuser for 2 months after January 14 and then cleaning it thoroughly on clear day March 14 2004 near noon, when irradiance level was high. We noted an upward step jump in measured voltages by +4%, that could explain, in part, observed long-term changes in UV-MFRSR throughput.

An independent on-site calibration method is useful to validate our calibration transfer from AERONET CIMEL instruments. In perfectly stable atmospheric conditions the Langley plot calibration method[17] would provide an independent check on the measurements, spectral band model, and $<V_0>$ calibrations. Standard Langley technique regresses $ln(V_n)$ versus m, so that $ln(Vo)$ is obtained as the zero-airmass intercept of a linear regression model given by equation (3). This method does not require any a-priori knowledge of the atmospheric transmittance beyond the stability requirement. However, the stability requirement is hard to meet at low-altitude sites, except for few exceptionally clear days in winter. To minimize aerosols affects, we tried to optimize standard the Langley technique by adjusting the regression time interval to ensure maximum possible stability of t_{ext} during calibration (see figure 7). We also applied an objective Langley analysis using the Harrison and Michalsky[17] program, which is the standard algorithm used in the USDA UVB shadowband network.

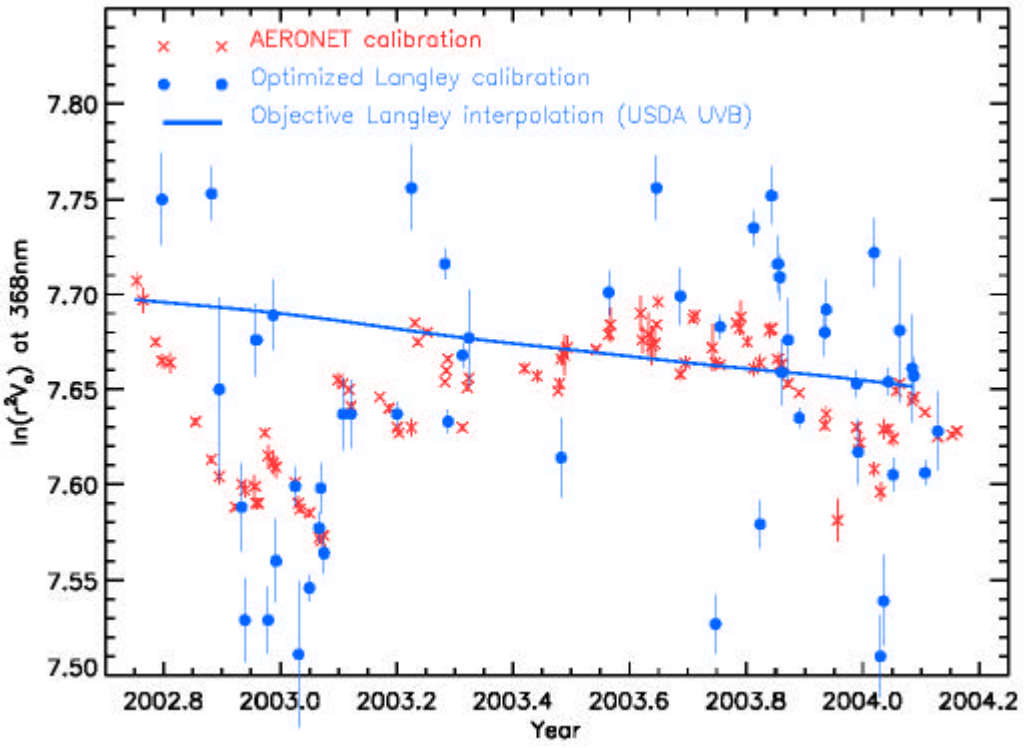

Figure 11. Langley calibration versus AERONET master instrument calibration at GSFC site.

Figure 11 shows the optimized on-site Langley technique C_o results (with 1-s_{Co} error bars). Both on-site Langley techniques produce significant day-to-day variations, but with the variations for the objective technique much larger. Only the optimized Langley technique tends to confirm the *Vo* time dependence seen from AERONET calibration, while the objective technique produces a relatively large range of values with no clear trend. Therefore, we only show time-interpolated results from the objective technique actually used in the USDA UVB shadowband network (solid curve in Figure 11). One can see that using only the objective Langley interpolated curve could produce errors in derived aerosol optical thickness up to 0.05 in worst conditions (in winter noon times with airmass m=2), while maximum τ error in summer is only ~0.02 (see equation (3)). We conclude that until UV-MFRSR seasonal *Vo* changes are better understood and corrected ~~for~~, independent long-term *Vo* calibration verification (CIMEL) is highly desirable for obtaining accurate aerosol retrievals

6. Conclusions

We demonstrated a new method of on-site UV-MFRSR relative calibration using co-located direct sun AERONET/CIMEL t_{ext} measurements and Langley Mauna Loa calibrations. The AERONET t_{ext} was interpolated or extrapolated to UV-MFRSR wavelengths and measurement time and used as input to UV-MFRSR spectral band model along with column ozone and surface pressure measurements to estimate UV-MFRSR zero air mass voltages, V_o. The method does not require stability of t_{ext} and allows independent V_o estimations for every 3-min measurement in each spectral channel. Daily average $<V_o>$ estimates were obtained for cloud-free conditions and compared with the on-site Langley plot technique. On the clearest stable days both calibration techniques agree within 1%. Uncertainties in CIMEL τ_{ext} measurements (using co-located backup reference CIMEL measurements) and in calibration transfer were considered as part of the combined UV-MFRSR V_o error budget.

Such comparisons provide an independent check of both instrument's radiometric and UV-MFRSR's angular calibration and allow precise tracking of the UV-MFRSR throughput changes (from possible diffuser contamination) by repeating the comparisons on clear days. We found relatively good $<V_o>$ reproducibility in summer (+/-2% in $<V0(368)>$), but larger than expected V_o changes in winter-fall seasons. The changes include periods of systematic day to day V_o decline for more than a month time periods (we identified 4 such periods with ~0.15%/day decline in V_o(368nm)) alternated with step jumps changes after major precipitation periods (rain or snow). The $<V_o>$ day-to-day changes were highly correlated in all UV-MFRSR channels, and possibly result from diffuser contamination and cleanings. Such V_o changes necessitate diffuser cleanings of stand-alone UV-MFRSR field instruments at least 2 times weekly or adding a quartz dome, which is less likely to absorb dirt particles.

Daily mean $<V_0>$ values were used to calculate τ_{ext} for individual 3-minute UV-MFRSR measurements (~5% outlier data rejection). These results compared well with interpolated AERONET τ_{ext} measurements (at 368nm daily rms differences in τ_{ext} were within 0.01 (1σ) for $\tau_{ext}< 0.4$ and within 0.02(1σ) for $\tau_{ext}<1.2$).

The essential advantage of the shadowband technique is that $<V_0>$ calibration obtained for direct-sun voltage can be applied to diffuse and total voltages to obtain total and diffuse atmospheric transmittances. These transmittances in combination with accurate t_{ext} data provide an essential foundation for the aerosol column absorption retrievals described in the second part of this paper.

References

1.O. Wild, X. Zhu, and M.J.Prather, " Fast-J: Accurate simulation of in- and below-cloud photolysis in tropospheric chemical models", *J. Atmos. Chem.,* **37**, 245-282, 2000.

2. M. Z. Jacobson, "Studying the effects of aerosols on vertical photolysis rate coefficient and temperature profiles over an urban airshed", *Journ. Geophys. Res.*, **103**, 10593-10604, 1998.

3. R.R. Dickerson, S. Kondragunta, G. stenchikov, K.L.Civerolo, B.G. Doddridge, and B.N.Holben, "The impact of aerosols on solar Ultraviolet radiation and photochemical smog", *Science* , 28, 827-830, 1997.

4. S. Madronich, *Environmental Effects of Ultraviolet (UV) Radiation*, chapter: UV radiation in the natural and perturbed atmosphere, *Lewis Publisher*, Boca Raton, 17-69, 1993.

5. M. Z. Jacobson, "Isolating nitrated and aromatic aerosols and nitrated aromatic gases as sources of ultraviolet light absorption", *Journ. Geophys. Res.*, **104**, 3527-3542, 1999.

6. N.A. Krotkov, P.K. Bhartia, J.R.Herman, V.Fioletov and J.Kerr, Satellite estimation of spectral surface UV irrdiance in the presence of tropospheric aerosols 1. Cloud-free case, *Journ. Geophys. Res*., 103, D8, 8779-8793, 1998.

7. A. Kylling, A. F. Bais, M. Blumthaler, J. Schreder, C.S. Zerefos, and E. Kosmidis, "Effect of aerosols on solar UV irradiances during the Photochemical activity and solar ultraviolet radiation campaign", *Journ. Geophys. Res.*, **103**, 26051-26060, 1998.

8. J. Reuder and H. Schwander, "Aerosol effects on UV radiation in nonurban regions", *Journ. Geophys. Res.*, **104**, 4065-4077, 1999.

9. J.R.Herman, N.Krotkov, E.Celarier, D.Larko, and G.Labow, "The distribution of UV radiation at the Earth's surface from TOMS measured UV-backscattered radiances," *J. Geophys. Res*., **104**, 12059-12076, 1999.

10. B. N. Wenny, V.K. Saxena, and J.E. Frederick, "Aerosol optical depth measurements and their impact on surface levels of ultraviolet-B radiation", *Journ. Geophys. Res.*, **106**, 17311-17319, 2001.

11. N.A. Krotkov, J.R.Herman, P.K. Bhartia, C. Seftor, Antti Arola, J. Kurola, S. Kalliscota, P. Taalas, I. Geogdzhaev, Version 2 TOMS UV algorithm: problems and enhancements, Opt. Eng. 41 (12) , 3028-3039, 2002.

12. N. A. Krotkov, J.R.Herman, P.K.Bhartia, C.Seftor, A.Arola, J.Kaurola, P.Taalas, I.Geogdzhaev, A. Vasilkov, OMI surface UV irradiance algorithm, P.Stammes (Ed.), vol. 3, ATBD-OMI_03, version 2, 2002 (http://eospso.gsfc.nasa.gov/eos_homepage/for_scientists/atbd/docs/OMI/ATBD-OMI-03.pdf).

13. J.L.Petters, V.K. Saxena, J.R. Slusser, B.N. Wenny, and S. Madronich, "Aerosol single scattering albedo retrieved from measurements of surface UV irradiance and a radiative transfer model", *Journ. Geophys. Res*, 108 (D9) 4288, doi:10.1029/2002JD002360, 2003.
14. V. Fioletov, J.B.Kerr, D.I.Wardle, N. Krotkov, J.R. Herman, "Comparison of Brewer ultraviolet irradiance measurements with total ozone mapping spectrometer satellite retrievals", *Opt. Eng*. **41** (12) 3051-3061, 2002.
15. D.S. Bigelov, J.R. Slusser, A. F. Beaubien, and J. R. Gibson, "The USDA ultraviolet radiation monitoring program", *Bull. Amer. Meteor. Soc.*, **79**, 601-615, 1998.
16. L. Harrison, J. Michalsky, and J. Berndt, "Automated Multi-Filter Rotating Shadowband Radiometer: An instrument for Optical Depth and Radiation Measurements", *Appl. Optics*, **33**, 5118-5125, 1994.
17. L. Harrison and J. Michalsky, "Objective algorithms for the retrieval of optical depths from ground-based measurements", *Appl. Optics*, **33**, 5126-5132, 1994.
18. B.N. Holben et al., "AERONET – A federated instrument network and data archive for aerosol characterization", *Remote Sensing Environment*, 66, 1-16, 1998.
19. B.N. Holben et al., "An emerging ground-based aerosol climatology: Aerosol Optical Depth from AERONET", *Journ. Geophys. Res.*, **106**, 12 067-12 097, 2001.
20. B. M. Herman, S.R. Browning, J.J.DeLuisi, "Determination of the effective imaginary term of the complex refractive index of atmospheric dust by remote sensing: The diffuse-direct radiation method", *J. Atm. Sciences*, **32**, 918-925, 1975.
21. King, M. and B.M. Herman, "Determination of the ground albedo and the index of absorption of atmospheric particles by remote sensing. Part I: Theory", *J.Atmos. Sciences*, **36**, 163-173, 1979.
22. M. King, "Determination of the ground albedo and the index of absorption of atmospheric particles by remote sensing. Part II: Application", *J.Atmos. Sciences*, **36**, 1072-1083, 1979
23. T. F. Eck, B.N. Holben, I. Slutsker, and Alberto Setzer, "Measurements of irradiance attenuation and estimation of aerosol single scattering albedo for biomass burning aerosols in Amazonia", *J. Geophys. Res*., **103**, 31865-31878, 1998.
24. T. F. Eck, B.N.Holben, D.E. Ward, O. Dubovik, J.S. Reid, A. Smirnov, M.M. Mukelabai, N.C. Hsu, N.T. O'NeilL, and I. Slutsker, "Characterization of the optical properties of biomass burning aerosols in Zambia during the 1997 ZIBBEE field campaign", *Journ. Geophys. Res*., **106**, D4, 3425-3448, 2001.
25. O. Dubovik and M.D. King, "A flexible inversion algorithm for retrieval of aerosol optical properties from Sun and sky radiance measurements", *J. Geophys. Res* ., **105**, D16, 20673-20696, 2000.
26. O. Dubovik, A. Smirnov, B.N. Holben, M. D. King, Y. J. Kaufman, T. F. Eck, and I. Slutsker, "Accuracy assessments of aerosol optical properties retrieved from Aerosol Robotic Network (AERONET) Sun and sky radiance measurements", *J Geophys. Res*., **105**, D8, 9791-9806, 2000.
27. O. Dubovik, B.Holben, T.Eck, A. Smirnov, Y. J. Kaufman, M. D. King, D. Tanre, and I. Slutsker, Variability of Absorption and Optical properties of key aerosol types observed in worldwide locations, *J. Atmos. Sciences*, **59**, 590-608, 2002.

28. J. Slusser, et al., “Comparison of column ozone retrievals by use of an UV multifilter rotating shadow-band radiometer with those from Brewer and Dobson spectrophotometers”, *Appl. Optics*, **38**, 1543-1551, 1999
29. T.F. Eck, B.N.Holben, J.S.Reid, O.Dubovik, A.Smirnov, N.T.O'Neill, I.Slutsker, and S.Kinne, Wavelength dependence of the optical depth of biomass burning, urban and desert dust aerosols, *Journ. Geophys. Res.*, **104**, 31333-31350, 1999.
30. A. Smirnov, B.N.Holben, T.F.Eck, O.Dubovik, and I. Slutsker, “Cloud screening and quality control algorithms for the AERONET data base”, *Rem. Sens. Env*., 73(3), 337-349, 2000
31. Herman, B. M., T. R. Caudill, D. E. Flittner, K. J. Thome, and A. Ben-David, A comparison of the Gauss-Seidel spherical polarized radiative transfer code with other radiative transfer codes, Appl. Opt, 34, 4563-4572, 1995.
32. J.R. Herman and E. Celarier, “Earth surface reflectivity climatology at 340 to 380 nm from TOMS data,” *J. Geophy. Res*., **102**, 28003-28011, 1997.
33. Leszscynski et al., “Erythemal weighted radiometers”, *Photochemistry and Photobiology*, **67**(2), 212-221, 1998.
34. J. Grobner, M. Blumthaler, and W. Ambach, “Experimental investigation of spectral global irradiance measurement errors due to a non ideal cosine response,” *Geophysical Research Letters*, **23**(18), 2493-2496, 1996.
35. G. E. Shaw, “Sun photometry”, *Bull Am. Meteorol. Soc.*,64,4-10, 1983
36. J. London, R.D.Bojkov, S.Oltmans, and J.I.Kelly, Atlas of the global distribution of total ozone July 1957-June 1967, *NCAR Tech. Note 133+STR*, 276 pp. NCAR, Colo., 1976.
37. S.C. Alfaro, S. Lafton, J.L.Rajot, P. Formenti, A. Gaudichet, and M.Maille, Iron oxides and light absorption by pure desert dust: An experimental study, *J. Geophys. Res., 109*, D08208, doi:10.1029/2003JD004374, 2004

Table 1 *UV-MFRSR measurement and correction errors***.**

Sources of measured errors in UV-MFRSR 368nm channel	τ=0.2		τ=0.8	
	θ=30	θ=70	θ=30	θ=70
	Measured signal, [mv]			
V_T, mv	1300	400	1100	300
V_D, mv	560	300	700	280
Diffuse fraction, DT	0.43	0.75	0.64	0.93
	Measurement errors, $s_{\ln V_T}$,[%]			
ΔlnVT: quantization	0.001	0.003	0.001	0.003
ΔlnVT: dark current	0.002	0.007	0.002	0.007
ΔlnVT: temperature	0.01	0.01	0.01	0.01
ΔlnVT: cosine correction	0.005	0.01	0.005	0.01
ΔlnVT: shadowing correction	0.01	0.01	0.01	0.01
Combined measurement error:	~0.018	~0.02	~0.025	~0.03

Table 2 *UV-MFRSR spectral band model*[1)]

Nominal band wavelength, nm[2)]	299.845	305.497	311.575	317.730	325.592	332.654	368.011
		UVB channels			UVA channels		
λ_{eff} [3)]	300.397	305.726	311.706	317.779	325.687	332.636	367.963
λ_{dir} [4)]	300.063	305.313	311.753	317.986	325.808	332.208	367.956
τ_{Ray} [5)]	1.216	1.128	1.031	0.947	0.854	0.786	0.5105
τ_{Ozone} [6)]	3.335	1.55	0.681	0.292	0.095	0.020	0.00007
$\tau_{Aerosol}$ [7)]	0.123	0.121	0.118	0.116	0.113	0.111	0.100
$<E_{TOP}>$, W/m2 [8)]	0.48	0.62	0.72	0.75	0.92	0.98	1.19
$<E_{BOT}>$, W/m2 [9)]	0.00004	0.002	0.02	0.05	0.11	0.16	0.35
Transmittance, $T_r=<E_{BOT}>/<E_{TOP}>$	0.0001	0.004	0.03	0.07	0.12	0.16	0.29

1) Example is given for 1 atm surface pressure, 350DU column ozone amount, and aerosol extinction optical thickness 0.1 at 368nm (Angstrom parameter α=1). Atmospheric transmittance is calculated for airmass m=2 (solar zenith angle 60^o).
2) Spectral response functions were measured by CUCF in air (September 2002). All wavelengths are shifted to vacuum wavelength scale
3) Channel weighted effective wavelength at the bottom of atmosphere
4) Equivalent monochromatic wavelength for direct irradiance at the bottom of atmosphere (equation (1))
5) Rayleigh scattering coefficients are based on the work by *Bates* [1984].
6) The high spectral resolution (~0.05 nm) ozone absorption coefficients are based on the laboratory measurements of *Bass and Paur* [1984]
7) Nominal aerosol model with $\tau_{ext}(368)$=0.1 and Angstrom parameter =1.
8) Extraterrestrial Solar Irradiance by ATLAS-3 SUSIM measurements convolved with UV-MFRSR SRF. This gives the absolute signal [Watts/m2], which would be measured in each UV-MFRSR channel at the top of atmosphere with diffuser oriented toward the Sun at 1AU
9) Direct normal absolute irradiance, which would be measured in each UV-MFRSR channel at the bottom of atmosphere with diffuser oriented toward the Sun at 1AU.

Table 3 *Calibration constants for AERONET CIMEL reference instruments at GSFC cite in 2002-2004. In the computation of* τ_{ext} *from direct Sun measurements, the Rayleigh optical depth is subtracted out from the total optical depth*[17-18]

Inst #	Start date at GSFC	End date at GSFC	ln(V0(after)/V0(before)) [1]		Central wavelength		Rayleigh subtraction	
			340	380	340	380	340	380
#94	12/16/03	Present	N/A	N/A	339.9	379.4	0.706	0.445
	05/13/03	06/17/03	-0.016 [6]	0.016 [6]	-"-	-"-	-"-	-"-
	12/18/02	02/03/03	-0.01 [3]	0.004 [3]	-"-	-"-	-"-	-"-
#89	10/17/03	12/15/03	N/A	N/A	339.9	380.1	0.706	0.442
	06/18/03	07/24/03	-0.022 [7]	-0.017 [7]	340.0	379.4	0.705	0.445
	09/28/02	12/17/02	0.005 [2]	0.004 [2]	-"-	-"-	-"-	- "-
#101	10/10/03	10/16/03	N/A	N/A	340.3?	380.2	0.706	0.445
	07/25/03	10/09/03	-0.007 [8]	-0.015 [8]	-"-	-"-	0.703	0.441
	03/14/03	05/12/03	-0.009 [5]	0.003 [5]	-"-	-"-	-"-	-"-
#37	02/04/03	03/13/03	N/A [4]	N/A [4]	340.3	380.5	0.703	0.440

1) *One set of Langley calibrations at Mauna Loa observatory (MLO) is done for AERONET reference instruments.*
2) *CIMEL #89 pre-deployment calibration on 09:09:2002, post-deployment calibration on 22:05:2003. Small increases in Vo with time (<0.5% between MLO calibrations) may possibly be due to uncertainty in the determination of Vo.*
3) *CIMEL #94 pre-deployment calibration on 15:11:2002, post-deployment calibration on 11:04:2003*
4) *CIMEL #37 - only had 1 calibration on 31:12:2002, data are being replaced with data from #89 and #94 for Feb 4 - Mar 14, 2003 for the level 2.0 data.*
5) *CIMEL #101 - pre-deployment calibration on 12:02:2003, post-deployment calibration on 02:07:2003*
6) *CIMEL #94 - pre-deployment calibration on 11:04:2003, post-deployment calibration on 25:08:2003*
7) *CIMEL #89 - pre-deployment calibration on 22:05:2003; post-deployment calibration on 06:10:2003*
8) *CIMEL #101 - pre-deployment calibration on 02:07:2003; post-deployment calibration on 09:12:2003*